applied sciences

MDPI

Article

Modelling and Numerical Simulation of Supercritical CO_2 Debinding of Inconel 718 Components Elaborated by Metal-Injection Molding

Aboubakry Agne * and Thierry Barrière

Femto-ST Institute, 24 rue de l'épitaphe, 25000 Besançon, France; thierry.barriere@univ-fcomte.fr
* Correspondence: aboubakry.agne@femto-st.fr; Tel.: +333-81-66-60-08

Received: 13 July 2017; Accepted: 29 September 2017; Published: 6 October 2017

Featured Application: The numerical simulation of the debinding step by using a supercritical fluid is used to predict the binder extraction to optimize the component's shape.

Abstract: A debinding step using the supercritical state of a fluid has been increasingly investigated for extracting organic binders from components obtained by metal-injection molding. It consists of placing the component in an enclosure subjected to pressure and temperatures higher than the critical point to perform polymer extraction of the Metal-injection molding (MIM) component. It is an alternative to conventional solvent debinding. The topic of this study is to model and simulate the supercritical debinding stage to elucidate the mechanism of polymer degradation and stabilization with a three-dimensional model. Modelling this extraction process would optimize the process on an industrial scale. It can be physically described by Fick's law of diffusion. The model's main parameter is the diffusion coefficient, which is identified by using linear regression based on the least-squares method. In the model, an effective length scale is specially developed to take into account the diffusion in all directions. The tests were performed for extracting polyethylene glycol, an organic additive, using supercritical CO_2 in injected components. The feedstock is composed of polypropylene, polyethylene glycol, and stearic-acid as binder mixed with Inconel 718 super-alloy powders. The identified parameters were used to calculate the diffusion coefficient and simulate the supercritical debinding step on the Comsol Multiphysics® finite-element software platform to predict the remaining binder. The obtained numerical simulation results are in good agreement with the experimental data. The proposed numerical simulations allow for the determination of the remaining polyethylene glycol (PEG) binder distribution with respect to processing parameters for components during the supercritical debinding process at any time. Moreover, this approach can be used in other formulation, powder, and binder systems.

Keywords: metal-injection molding; debinding; simulation; supercritical

1. Introduction

Metal-injection molding (MIM) is a process used to obtain complex net shape components with accurate final tolerances and surface roughness [1,2]. It consists of preparing high-loaded mixtures with metallic powders (feedstock) and thermoplastic polymers (multi-component binder). The feedstock undergoes three stages: injection molding, debinding, and sintering [3]. The MIM process presents some interesting properties for the industrial mass production of complex-shaped components.

The feedstock behavior (binder-weight fraction, powder-volume loading, critical-volume loading, chemical composition, shear-viscosity behavior, etc.) has an important influence on the final components [4]. Therefore, as important features of the process, the mixing conditions and thermal-physical characteristics must be identified [5]. The binder must support the powder load

and carry the powder into the mold cavity during the injection-molding step [6]. It should interact well with the metal powders [5]. Then, the binder is removed during the debinding step, and finally sintered by solid-state diffusion of the powder to obtain the final dense metallic component, which has mechanical properties similar to those of a wrought material [7].

The debinding stage, corresponding to the extraction of the binder, is probably the most time-consuming step. In addition, it is difficult to completely remove the binder without introducing defects into the component [8]. Different methods can be used to accomplish the debinding process [9,10]. The most common debinding techniques are thermal debinding [11], catalytic debinding [12], and solvent debinding [13].

Catalytic debinding focuses on a solid-to-vapor catalytic degradation, e.g., exposing an acetyl-based component to acid vapors [12]. It results in a much faster binder removal and a higher handling strength than thermal debinding [14]. However, this method can affect the chemical properties of the powder skeleton.

Thermal debinding involves the oxidation of the binder in air, or pyrolysis in nitrogen [9]. During thermal debinding, the component is heated until the degradation temperature of the main binder (backbone). The advantage of this process is that the main binder is removed without disrupting the packing of the powder particles. However, if the binder oxidation is incomplete, the residue may affect the final properties of the component [15]. Moreover, the high debinding stress can affect the final shape. To reduce defects during this step, some alternative methods have been developed.

Solvent debinding consists of extracting a soluble binder by immersing the component in a solvent (e.g., water or ethanol) before the thermal debinding [6,16–18]. Organic solvents are commonly used and have the advantages of shape retention and rapid debinding [8]. However, water is often used because it is less pollutant and more economic. However, the diffusion time of a soluble binder during water debinding is much longer. A shorter and innovative method for extracting an organic binder is to use supercritical fluid debinding [19–22]. Supercritical debinding was reported by Chartier et al. [23] in 1995 on ceramic-powder components. It has proven to be a useful alternative to solvent debinding; it reduces the debinding time and eliminates defects in green-body components [22]. Carbon dioxide is the most used fluid because it is very effective and environmentally friendly [19]. Nevertheless, during supercritical debinding, the component is subjected to high pressure, which can cause additional shrinkage. The main goal of these methods is to make the component porous before the thermal degradation of the binder.

The relevant properties of a supercritical fluid are the density, the viscosity, the mass diffusivity, and the thermal conductivity, as reported by Avelino et al. [24]. These properties can be easily controlled by the pressure and the temperature of the supercritical fluid. Moreover, the supercritical state of carbon dioxide is easily obtained (pressure up to 30 MPa and temperature up to 373 K). Chartier et al. [25] described two mechanisms involved during the supercritical debinding of organic polymers in a solid state: the solubilization of the polymer molecules, and the diffusion of the solubilized species.

Various models have been developed to predict the debinding time and the degradation kinetics of the binders, adapted to available extraction methods [9,25–27]. Chartier et al. [25] developed a model using the diffusion principle to determine the accurate extraction kinetic of a soluble solid organic binder during supercritical debinding. Their model was in good agreement with the experimental results for paraffin extraction. Unfortunately, their model was not adapted to liquid binders and had to be completed with capillary migration. Moreover, the diffusion coefficient was identified at each debinding time and pressure. There were many variables for parameter identification and the model was evaluated on bar specimens.

Modelling condensed-solvent debinding, using the diffusion principle to predict the removal of organic binders contained in components produced by MIM, was also previously studied by German et al. [28]. They considered that the soluble binder dissolved into the solvent and then diffused to the compact surface, where it was removed. Their model was based on Fick's diffusion law. They considered that the main step of the debinding process is the interdiffusion of the solvent

and binder within the compact. Using linear regression on the experimental results and considering diffusion along one direction, the coefficient was identified as the temperature function. Their method made it possible to easily identify the main parameter of the diffusion model: the diffusion or interdiffusion coefficient. It was used in our current study to predict the binder extraction with a supercritical fluid.

There is a lack of simulations of PEG extraction of a feedstock composed of a super-alloy powder during supercritical debinding, and existing models are insufficient for clearly identifying the main parameters affecting the component shapes. Thus, one of the major objectives and the highlight of this investigation is to identify the diffusion coefficient from the solvent-debinding model investigated by German et al. [28] and to use it to predict binder extraction through numerical simulations. This is because the two debinding techniques, solvent and supercritical fluid debinding, use the same extraction mechanism: Diffusion of the solution binder/solvent from the interior to the external surfaces of the component [16,25]. The method applied Fick's second law, which expresses a linear relation between the mass flow and the concentration gradient. The effective length scale presented by German et al. [29] to consider the component shape is given by the volume to surface area ratio of a component. It was used in this current study to consider all directions during the diffusion in a cylindrical component. The numerical simulation of the debinding step using supercritical CO_2 with the Comsol Multiphysics® finite-element software platform was performed to predict the PEG binder distribution and the degradation or removal from the component, and to optimize the component design before the debinding stage. The model's main parameter is the diffusion coefficient, which was identified with experimental data obtained from supercritical CO_2 debinding at three different temperatures. The simulation of the process is used to validate the model that describes the binder extraction. Moreover, various experimental tests of supercritical debinding at different debinding times were carried out on injected components. The numerical and experimental results were compared.

2. Materials and Methods

This study used Inconel 718 metallic powder which is a nickel-based super-alloy was provided by Sandvik Osprey Powders (Neath, UK). The Inconel powder's volume loading is equal to 60% (92 wt %). Its chemical composition is presented in Table 1. The metal-powder particles obtained by atomization with water have a spherical shape and a diameter d_{90} of less than or equal to 32 µm. Inconel is being investigated more and more as a structural alloy for producing aeronautic components by metal-injection molding because of its higher resistance to oxidation, excellent performance at high temperatures (high strength up to 1400 °C), and its impact strength [30,31].

Table 1. Chemical composition in mass percentage of the Inconel 718.

Ni	Fe	Cr	Nb	Mo	Ti	Al	C
52.5	19.0	19.0	5.3	3.0	0.9	0.5	0.0

The components' multi-component binder is usually composed of three different ingredients (surfactant, rheofluidifiant, the rigidifying, etc.) [6]. This study used the binder formulation previously investigated by Royer et al. [6]. The multi-component binder volume is composed of 16% polypropylene (PP) provided by Sabic (Paris, France), 22% polyethylene glycol (PEG), and 2% stearic acid (SA) purchased from EMD Millipore Corporation (Billerica, MA, USA). The PP strengthens the injected components to rigidify the green-part structure and allow for manipulation after debinding. The PEG, which is a water soluble polymer, gives the binder fluidity during the injection step. The SA is a long-chain polymer that prevents the metallic powders from aggregating, to assure some homogeneity inside of the feedstock. The characteristics of the binder components and their weight fractions are given in Table 2.

Table 2. Characteristics of polymer binders used in the present study.

Polymer	Weight Fraction, %	Density, g/cm^3	Melting Point, K
PP	2.68	0.90	418
PEG	4.95	1.21	335
SA	0.35	0.94	341

The elaborated feedstock was assembled in a twin-screw Brabender mixer provided by Brabender GmbH & Co. KG (Duisburg, Germany) with a 50-cm^3 mixing chamber; it can reach a maximum temperature of 773.15 K. It consists of two screws that are especially adapted for highly loaded mixtures with metallic powders. The powder and binder were mixed for 45 min at 30 rpm and 443.15 K. After blending the feedstock, the injection-molding process was performed using an Arburg 220S hydraulic injection-molding press provided by ARBURG GmbH & Co KG (Lossburg, Germany) equipped with a cylindrical mold cavity with an injection volume between 3 and 12 cm^3.

The equipment dedicated to the MIM process has an anti-abrasive and bi-metallic single-screw barrel with a 15-mm diameter and a 600-mm length. The maximal injection pressure can reach 250 MPa. The maximum injection temperature was 673.15 K and the maximum injection flow was approximately 22 cm^3/s. The injection pressure was 180 MPa, and the temperatures of the injected feedstocks and the die-cavity mold were 443.15 K and 318.15 K, respectively. The specimens used for the supercritical debinding were 15-mm long with a diameter of 10 mm. The weights of the injected cylindrical specimens had a mean deviation of 0.2 g; thus, showing the good homogeneity of the injected components, see Figure 1.

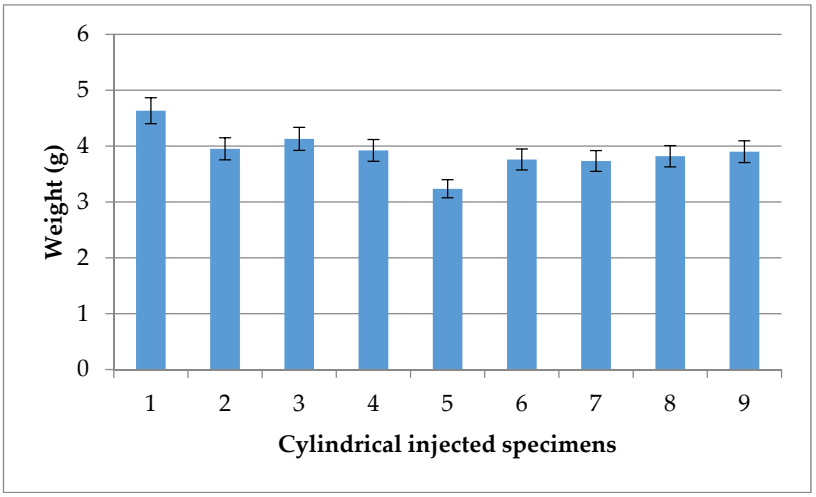

Figure 1. Weight evolution for the injected specimens obtained by an injection-molding process (15-mm length and 10-mm diameter).

During the debinding step using supercritical CO_2 equipment provided by SEPAREX Supercritical Fluid Technology S.A. (Champigneulles, France), the components were placed in a temperature and pressure-controlled enclosure under a CO_2 flow. Before starting the debinding process for each temperature condition, the components were weighed and inserted in the autoclave under environmental conditions. As shown in the Figure 2a, gaseous carbon dioxide (1) is extracted from the bottle by a valve (2) at the beginning of the process. It is then cooled to a liquid state (3) and directed towards a pump (4) that controls the pressure. When it reaches the pressure needed for a supercritical state (up to the critical point, see Figure 2b), the carbon dioxide is heated by a heat exchanger (5). At the supercritical state, the CO_2 is directed towards the autoclave (6), which contains the components (7). Then, thermocouples are used to control the temperature (8). The carbon dioxide is recovered

(9), cooled, and directed towards a recycling line (3). At the end of the process, the components are weighed again to estimate the quantity of PEG removed. Three successive tests were performed for each debinding temperature. A diagram of the equipment setup is shown in Figure 2a.

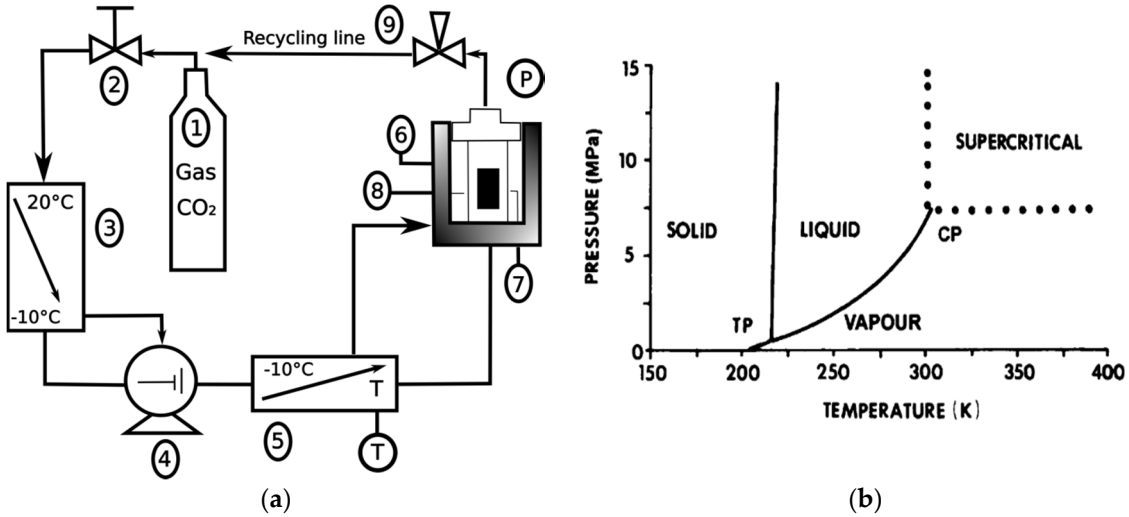

Figure 2. (**a**) Diagram of the supercritical debinding equipment [10]; (**b**) Carbon dioxide pressure-temperature phase diagram, showing the triple point (TP) and critical point (CP) [32].

Royer et al. [6] identified the optimal supercritical debinding kinetics as 40 MPa and 423.15 K to remove 100% of the PEG, with a molar weight of 20,000 g/mol, from the injected components in four hours. Knez et al. [33] reported that the density of the PEG/CO_2 binary solution increased with an increasing pressure, and the molecular weight of the polymer had a slight effect on the density of the binary system. In this study, the cylindrical components were debound at an optimal pressure of 40 MPa over four hours at three different temperatures: 383.15 K, 403.15 K, and 423.15 K. It is supposed that the mass loss is totally due to the PEG extraction. To quantify the extraction kinetic, three tests at two different time steps (1 h and 2 h) under optimal conditions (423.15 K and 40 MPa) were conducted.

3. Results and Discussion

3.1. Supercritical Debinding

Figure 3 shows the weight fraction of the PEG extracted in four hours after being debound by supercritical carbon dioxide at 40 MPa, and the temperatures from 383.15 to 483.15 K. The results indicate that the discrepancies between the three repetitive tests for all of the temperatures were approximately 1.5%.

It is observed that the evolution of the PEG binder removal is proportional to the temperature. When the temperature increases, the PEG removal increases. The temperature is an influential parameter on the debinding. The plasticizing effect of the supercritical carbon dioxide probably affects the melting point of the binder system [22]. The effect of the optimal supercritical debinding parameters (T = 423.15 K and P = 40 MPa) on the components' deformation after the debinding tests was lower than 1%. Moreover, the PEG was entirely extracted with 423.15 K and 40 MPa after four hours. The parameter identification of Fick's model will be carried out with this experimental database.

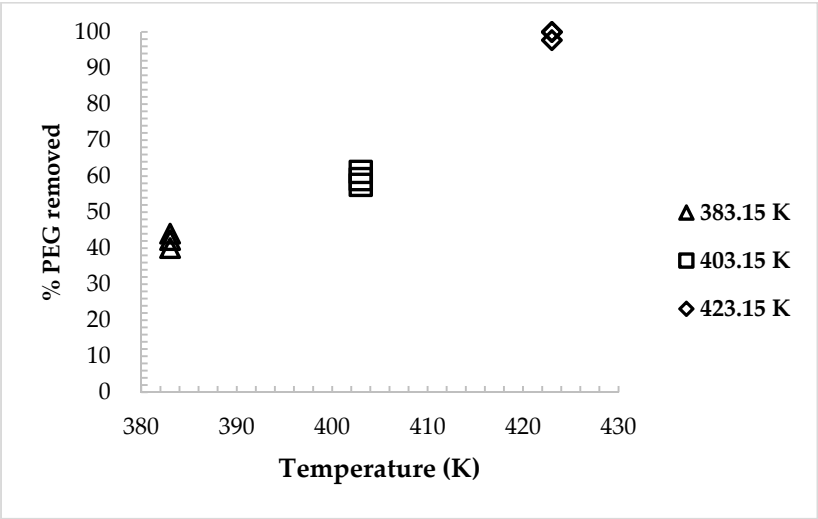

Figure 3. Removed weight fraction of polyethylene glycol (PEG) versus the temperature in cylindrical components after debinding by supercritical carbon dioxide (CO_2) under 40 MPa for four hours.

3.2. Process Modelling

During the debinding step, the supercritical CO_2 diffuses in the component and its molecules create chains with the organic binder, which then diffuses from the center to the outer surfaces of the component [25]. The solubilization of the binder molecules and the diffusion of the solution are the two main mechanisms of supercritical debinding. If one considers the high solubility of the soluble binder in a supercritical fluid, the only stage that controls the extraction by solvent likely remains the diffusion [25]. The extraction or diffusion rate of soluble polymers in a supercritical fluid using the concentration field can be modelled by a one-dimensional diffusion mass, which is described by Fick's diffusion law [10,25,34] as:

$$\frac{\partial C}{\partial t} = D\left(\frac{\partial^2 C}{\partial x^2}\right), \tag{1}$$

where t is the debinding time, C is the concentration of the diffusing substance, x is the normal direction to the section (diffusion direction), and D is the diffusion coefficient of the solute, which is expressed as:

$$D = D_o \exp\left(\frac{-E}{kT}\right), \tag{2}$$

where D_o is a pre-exponential factor that represents the diffusivity frequency, E is the activation energy in kJ/mol, k is the Boltzmann constant and T is the temperature in Kelvin.

3.3. Boundary and Initial Conditions

It is assumed in the model that the concentration of the soluble polymers at the outer surfaces is always zero; indeed, they are debound (hydrated) at the beginning of the process [28]. When considering the diffusion along a cylindrical component, the equation can be solved by applying the following initial boundary conditions, i.e., a $2L$ slab length ($-L$ to L), with one end and its surfaces sealed (support):

$$C = C_o, \text{ for } 0 < x < L \text{ at } t = 0 \tag{3}$$

$$C = C_l = 0, \text{ for } x = L \text{ at } t > 0 \tag{4}$$

$$\frac{\partial C}{\partial x} = 0, \text{ for } x = 0 \text{ at } t \geq 0. \tag{5}$$

3.4. Parameter identification

German et al. [29] introduced an effective length scale ψ that considered the component's shape and dimensions during solvent debinding. For a long solvent duration or supercritical fluid debinding ($t >> 0$), and introducing the effective length scale for a cylinder, the fraction of the remaining soluble polymer can be approximately expressed as:

$$F = \frac{C_a}{C_i} = \exp\left(-\frac{Dt\pi^2}{\psi^2}\right), \tag{6}$$

$$\psi = \frac{\pi d^2 \frac{L}{4}}{\pi D\left(L + \frac{d}{2}\right)}, \tag{7}$$

where C_a is the average concentration during the extraction, C_i is the initial concentration, and d is the diameter of the cylindrical component. Introducing the diffusion coefficient D, Equation (6) can be expressed as a linear relationship:

$$\ln(-\ln(F)) = \ln\left(\frac{D_o t\pi^2}{\psi^2}\right) - \left(\frac{E}{k}\right)\left(\frac{1}{T}\right), \tag{8}$$

Figure 4 shows a plot of $\ln(-\ln(F))$, according to the inverse of the temperature *(1/T)*. Considering that the diffusivity of the solute at each temperature is constant [20], a linear regression using an ordinary least-squares method was conducted to minimize the sum of squared differences between the observed and predicted values. It was used to identify the diffusion coefficient as a function of the temperature. An apparent activation energy E of 20 kJ/mol and a pre-exponential factor D_o of 2.4×10^{-3} were identified from the linear regression, shown in Figure 4, with $\psi^2 \approx 2.8$ mm^2 calculated from Equation (7).

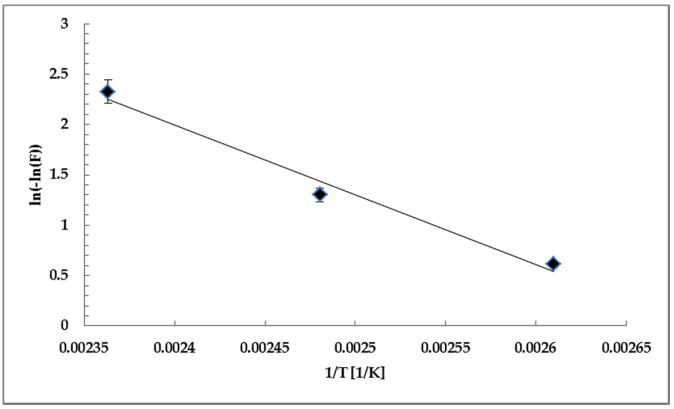

Figure 4. Temperature dependence and linear regression of PEG extraction after four hours' supercritical debinding under 40 MPa.

The diffusion coefficient D is calculated with Equation (2) using the identified activation energy and the pre-exponential factor. For a supercritical debinding at 423.15 K at 40 MPa, the diffusion coefficient D is equal to 7.46×10^{-6} cm^2/s. This value is lower than the diffusion coefficient identified by Chartier et al. [25], which was 9.5×10^{-6} cm^2/s for paraffin-wax extraction from ceramic components under 28 MPa at 345.15 K. The diffusion coefficient depends on the component shape, the powders' volume loading, and the powder size. The PEG used in this study has a high molar weight. The calculated diffusion coefficient is used for the numerical simulations of the supercritical debinding stage to predict the PEG removed from a cylindrical component.

3.5. Numerical Simulations of Supercritical Debinding

The numerical simulations were run using the Comsol Multiphysics® finite-element software platform version 5.2 developed by Comsol Inc. (Burlington, MA, USA) in 2015. The main objective was to use Fick's model and the identified coefficient to confront the experimental and numerical results of the weight loss during the PEG extraction by supercritical CO_2 in an injected component. The chemical module transfer of the software species was used to simulate the mass transport and chemical reactions in various environments. The transport interface of the diluted species was also used to estimate the concentration of an aqueous solution in a solvent. When working with the numerical solution of any time-dependent problem, a very costly part is assembling the finite-element matrix at each time step [35]. In this study, the following simplifying hypotheses are assumed for the physical model:

- the component is continuous;
- the soluble polymer (PEG) is distributed homogeneously in the component;
- PEG is the only soluble binder;
- the weight loss is only due to the dissolution and elimination of the soluble binder;
- there is no interaction between the other binder constituents (PP, SA) contained in the component; and,
- there is no temperature variation during the supercritical debinding.

The solution to the problem requires initial boundary conditions. Initially, the concentration C_i, which represents the average molar concentration of PEG in the injected components, is equal to 1.3×10^{-2} mol/m^3. To simplify the numerical results' interpretation, the relative value of the concentration, which includes 100% PEG initially in the component, was used. The diffusion coefficient identified previously was used ($D = 7.46 \times 10^{-6}$ cm^2/s). During the debinding by the supercritical fluid (CO_2), two boundary conditions existed. One was the impermeable surface, which represents the end of the cylindrical component (support). The outer surfaces, which are exposed to the supercritical CO_2, have a concentration C_o equal to zero:

- $\frac{\partial C}{\partial x} = \frac{\partial C}{\partial y} = \frac{\partial C}{\partial z} = 0$ for $x = 0$ at $t \geq 0$;
- $C = C_o = 0$ for outer surfaces at $t = 0$;
- $C = C_i = 100\%$ at $t = 0$.

A cylindrical component with length $L = 15$ mm and diameter $d = 10$ mm, as shown in Figure 5, was modelled in three dimensions (3D) by the finite-elements method (FEM) and simulated using the various modules described previously. The debinding time retained for this simulation was four hours, like the experimental debinding. The 3D domain was discretized using an automatic mesh generator with 77,645 linear tetrahedral elements with four nodes. A convergence test, which is not detailed in this study, validated the mesh quality. An explicit time-stepping scheme was used for the time-dependent solver algorithm. The solution is given each minute until the entire process reaches $t = t_f = 4$ h.

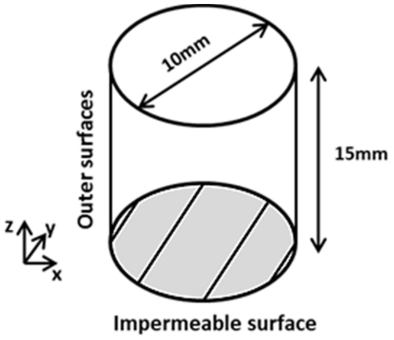

Figure 5. Description of three-dimensional geometry used for finite-elements method (FEM) simulation with boundary conditions.

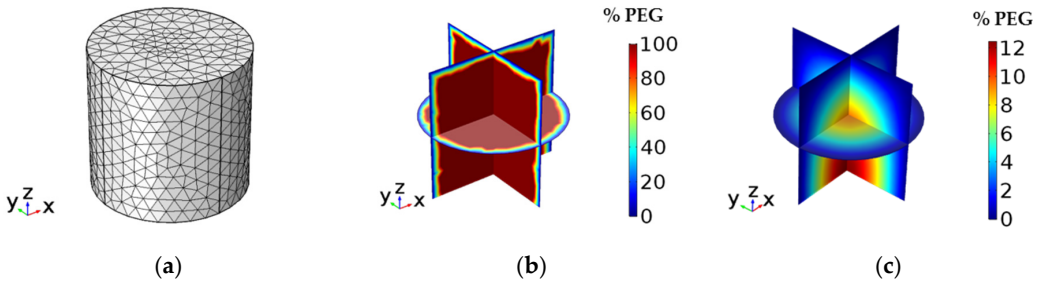

Figure 6. Numerical results according to a multi-slice view: (**a**) 3D model meshed by FEM; (**b**) initial stage (t = 0); and (**c**) final stage (t = 4 h) of the PEG binder distribution during debinding by supercritical CO_2 under 40 MPa and 423.15 K.

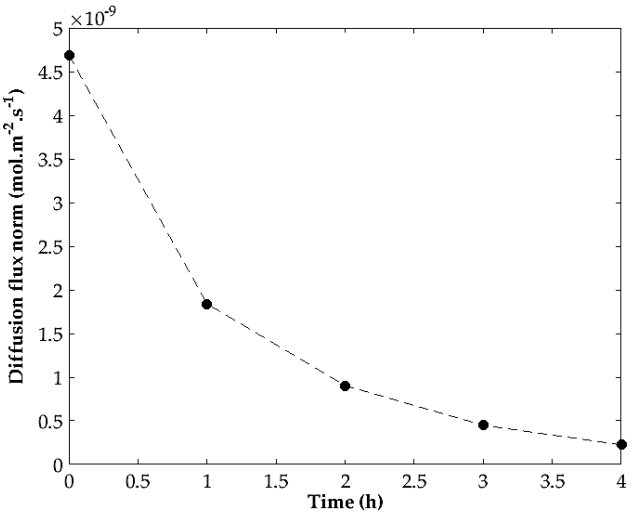

Figure 7. Diffusion flux norm from numerical simulation results vs. debinding time during supercritical CO_2 under 40 MPa and 423.15 K.

Numerical simulations were carried out on the PEG distribution during the debinding step using supercritical CO_2 on an injected cylindrical component with a powder-volume loading equal to 60%, for various debinding kinetics in terms of temperature and time parameters. As mentioned above, the binder system is composed of PP, SA, and PEG, which is the soluble binder. Figure 6 shows the remaining PEG distribution in the cylindrical component during the debinding by supercritical CO_2, according to a multi-slice view from the initial time (t = 0) to the final stage (t = 4 h). It is evident that the binder remains from the component's center to its outer surfaces during the debinding. The obtained results show an isotropic diffusion, and at the final stage the binder is present in the component's center. This is due to the diffusion flux, which was high at the beginning of the debinding and decreased rapidly during the extraction process, according to Figure 7. However, to improvements in the debinding time, the component's position can be changed in the enclosure during supercritical debinding to reduce the impermeable surface in order to increase the diffusion flux.

Figure 8 compares the remaining PEG during the numerical simulation of the supercritical debinding and the experimental results at different debinding times. The model correctly reproduces the experimental conditions because the experimental results are in good agreement and correspond with the mean value of the three tests performed at one and two hours under optimal conditions. The PEG extraction rate increased rapidly at the beginning of the debinding, showing an exponential extraction. At the final stage of the experiment, the remaining PEG was equal to 100%. The numerical simulation predicted 95% of PEG to remain at the final stage. It was necessary to add a half hour to remove all of the binder due to the low diffusion flux norm, numerically. The numerical simulation

results showed an excellent agreement with the experimental database. This minor discrepancy is probably due to the assumption of an impermeable surface on the cylindrical component.

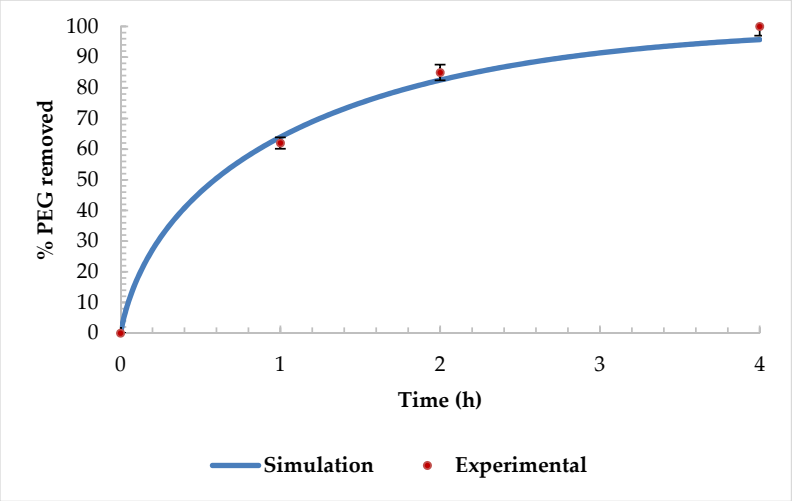

Figure 8. Predicted PEG removed from numerical simulation and experimental results versus debinding time during supercritical CO_2 under 40 MPa and 423.15 K.

4. Conclusions

Experimental investigations and numerical simulations related to the debinding stage by supercritical carbon dioxide were carried out for cylindrical components obtained by a metal-injection molding process with Inconel 718 super-alloy powders. Experimental results showed that the supercritical debinding was very efficient because PEG, which is an organic binder, was fully extracted with an optimal kinetic rate (in four hours under 40 MPa at 423.15 K). Three tests were performed at different times under optimal conditions in order to ensure the repeatability of the process and a mean value during parameter identification. The results showed an exponential evolution of the PEG extraction over time during the process.

A model based on Fick's law was used to describe the diffusion during the debinding. The effective length scale was introduced in the model to take into account the cylindrical shape of the components during the supercritical debinding. It was successfully estimated and used for the parameter identification for the cylindrical shape. These results can be used for more complex shape components in industrial applications. This has not been the case with previous supercritical debinding models.

The diffusion coefficient, which controls the debinding rate, was identified using the linear-regression method with the experimental values under optimal pressure. The identified coefficient was used for the numerical simulation of the dissolved PEG in MIM components during the supercritical debinding at 423.15 K under 40 MPa. The PEG removal values from the numerical results were compared to those from the experimental tests at three different debinding times. The results obtained with our implemented three-dimensional model were in proper agreement with the experimental ones. Using the present model to identify the diffusion coefficient and to simulate with finite-element software, one can properly analyze the distribution of the remaining binder content and the extraction rate from the initial to final stage of supercritical fluid debinding of the MIM component.

The proposed numerical simulations allow for the determination of the binder distribution of the remaining PEG versus processing parameters in components during the supercritical debinding process at any time. Such a model might also be suitable for other feedstocks if the appropriate coefficients are selected. The procedure proposed in this study represents the overall experimental data; thus, it can be readily employed in the numerical modelling of the overall sequential and global optimization associated with the powder injection-molding process.

Acknowledgments: The authors wish to thank the Regional Council of Franche-Comté and the FUI PROPIM project for the financial support and supercritical equipment within the framework of the MIFHYSTO Equipex platform.

Author Contributions: Modelling and numerical simulation were developed by Aboubakry Agne. Thierry Barrière has participated to the results discussion and the experimental procedure.

Conflicts of Interest: The authors declare no conflict of interest.

References

1. German, R.M. Injection Molding of Metals and Ceramics. *Met. Powder Ind. Fed.* **1997**, *3*. [CrossRef]
2. Wolff, M.; Schaper, J.G.; Suckert, M.R.; Dahms, M.; Feyerabend, F.; Ebel, T.; Willumeit-Römer, R.; Klassen, T. Metal Injection Molding (MIM) of Magnesium and Its Alloys. *Metals* **2016**, *6*, 118. [CrossRef]
3. Fang, W.; He, X.; Zhang, R.; Yang, S.; Qu, X. Evolution of stresses in metal injection molding parts during sintering. *Trans. Nonferrous Met. Soc. China* **2015**, *25*, 552–558. [CrossRef]
4. Romero, A.; Herranz, G. Development of feedstocks based on steel matrix composites for metal injection moulding. *Powder Technol.* **2017**, *308*, 472–478. [CrossRef]
5. Lin, D.; Sanetrnik, D.; Cho, H.; Chung, S.T.; Kwon, Y.S.; Kate, K.H.; Hausnerova, B.; Atre, S.V.; Park, S.J. Rheological and thermal debinding properties of blended elemental Ti-6Al-4V powder injection molding feedstock. *Powder Technol.* **2017**, *311*, 357–363. [CrossRef]
6. Royer, A.; Barrière, T.; Gelin, J.-C. Development and Characterization of a Metal Injection Molding Bio Sourced Inconel 718 Feedstock Based on Polyhydroxyalkanoates. *Metals* **2016**, *6*, 89. [CrossRef]
7. Valencia, J.; Spirko, J.; Schmees, R. Sintering Effect on the Microstructure and Mechanical Properties of Alloy 718 Processed by Powder Injection Molding - Superalloys. *Superalloys 718 625 706 Var. Deriv. Ed. EA Loria Miner. Met. Mater. Soc.* **1997**, *1997*, 753–762.
8. Chen, G.; Cao, P.; Wen, G.; Edmonds, N. Debinding behaviour of a water soluble PEG/PMMA binder for Ti metal injection moulding. *Mater. Chem. Phys.* **2013**, *139*, 557–565. [CrossRef]
9. Belgacem, M.; Thierry, B.; Jean-Claude, G. Investigations on thermal debinding process for fine 316L stainless steel feedstocks and identification of kinetic parameters from coupling experiments and finite element simulations. *Powder Technol.* **2013**, *235*, 192–202. [CrossRef]
10. Chartier, T.; Ferrato, M.; Baumard, J.F. Supercritical debinding of injection molded ceramics. *J. Am. Ceram. Soc.* **1995**, *78*, 1787–1792. [CrossRef]
11. Hwang, K.S.; Tsou, T.H. Thermal debinding of powder injection molded parts: Observations and mechanisms. *Metall. Trans. A* **1992**, *23*, 2775–2782. [CrossRef]
12. Bloemacher, M.; Weinand, D. CatamoldTM-a new direction for powder injection molding. *J. Mater. Process. Technol.* **1997**, *63*, 918–922. [CrossRef]
13. Kim, S.W.; Lee, H.-W.; Song, H.; Kim, B.H. Pore structure evolution during solvent extraction and wicking. *Ceram. Int.* **1996**, *22*, 7–14. [CrossRef]
14. Gonzalez-Gutierrez, J.; Stringari, G.; Emri, I. Powder Injection Molding of Metal and Ceramic Parts. In *Some Critical Issues for Injection Molding*; InTech: Rijeka, Croatia, 2012.
15. Masia, S.; Calvert, P.D.; Rhine, W.E.; Bowen, H.K. Effect of oxides on binder burnout during ceramics processing. *J. Mater. Sci.* **1989**, *24*, 1907–1912. [CrossRef]
16. Yang, W.-W.; Yang, K.-Y.; Wang, M.-C.; Hon, M.-H. Solvent debinding mechanism for alumina injection molded compacts with water-soluble binders. *Ceram. Int.* **2003**, *29*, 745–756. [CrossRef]
17. Hwang, K.S.; Hsieh, Y.M. Comparative study of pore structure evolution during solvent and thermal debinding of powder injection molded parts. *Metall. Mater. Trans. A* **1996**, *27*, 245–253. [CrossRef]
18. Enneti, R.K.; Shivashankar, T.S.; Park, S.-J.; German, R.M.; Atre, S.V. Master debinding curves for solvent extraction of binders in powder injection molding. *Powder Technol.* **2012**, *228*, 14–17. [CrossRef]
19. Nalawade, S.P.; Picchioni, F.; Janssen, L.P.B.M. Supercritical carbon dioxide as a green solvent for processing polymer melts: Processing aspects and applications. *Prog. Polym. Sci.* **2006**, *31*, 19–43. [CrossRef]
20. Kim, Y.-H.; Lee, Y.-W.; Park, J.-K.; Lee, C.-H.; Lim, J. S. Supercritical Carbon Dioxide debinding in metal injection molding (MIM) process. *Korean J. Chem. Eng.* **2002**, *19*, 986–991. [CrossRef]

21. Kim, S.W. Debinding behaviors of injection molded ceramic bodies with nano-sized pore channels during extraction using supercritical carbon dioxide and n-heptane solvent. *J. Supercrit. Fluids* **2010**, *51*, 339–344. [CrossRef]
22. Chartier, T.; Bordet, F.; Delhomme, E.; François Baumard, J. Extraction of binders from green ceramic bodies by supercritical fluid: influence of the porosity. *J. Eur. Ceram. Soc.* **2002**, *22*, 1403–1409. [CrossRef]
23. Chartier, T.; Ferrato, M.; Baumard, J.-F. Influence of the debinding method on the mechanical properties of plastic formed ceramics. *J. Eur. Ceram. Soc.* **1995**, *15*, 899–903. [CrossRef]
24. Avelino, H.M.N.T.; Fareleira, J.M.N.A.; Gourgouillon, D.; Igreja, J. M.; Nunes da Ponte, M. Viscosity of poly(ethyleneglycol) 200 [PEG 200] saturated with supercritical carbon dioxide. *J. Supercrit. Fluids* **2017**, *128*, 300–307. [CrossRef]
25. Chartier, T.; Delhomme, E.; Baumard, J.-F. Mechanisms of Binder Removal Involved in Supercritical Debinding of Injection Moulded Ceramics. *J. de Physique III* **1997**, *7*, 291–302. [CrossRef]
26. Zhu, B.; Qu, X.; Tao, Y. Mathematical model for condensed-solvent debinding process of PIM. *J. Mater. Process. Technol.* **2003**, *142*, 487–492. [CrossRef]
27. Krauss, V.A.; Oliveira, A.A. M.; Klein, A.N.; Al-Qureshi, H.A.; Fredel, M.C. A model for PEG removal from alumina injection moulded parts by solvent debinding. *J. Mater. Process. Technol.* **2007**, *182*, 268–273. [CrossRef]
28. German, R.M.; Lin, S.T. Extraction Debinbding of Injection Molded Parts by Condensed Solvent. *Powder Metall. Int.* **1989**, *21*, 19–24.
29. Shivashankar, T.S.; German, R.M. Effective Length Scale for Predicting Solvent-Debinding Times of Components Produced by Powder Injection Molding. *J. Am. Ceram. Soc.* **1999**, *82*, 1146–1152. [CrossRef]
30. Özgün, Ö.; Gülsoy, H.Ö.; Yılmaz, R.; Fındık, F. Microstructural and mechanical characterization of injection molded 718 superalloy powders. *J. Alloys Compd.* **2013**, *576*, 140–153. [CrossRef]
31. Özgün, Ö.; Özkan Gülsoy, H.; Yilmaz, R.; Findik, F. Injection molding of nickel based 625 superalloy: Sintering, heat treatment, microstructure and mechanical properties. *J. Alloys Compd.* **2013**, *546*, 192–207. [CrossRef]
32. Mendes, R.L.; Nobre, B.P.; Cardoso, M.T.; Pereira, A.P.; Palavra, A.F. Supercritical carbon dioxide extraction of compounds with pharmaceutical importance from microalgae. *Protag. Chem. Frausto Silva* **2003**, *356*, 328–334. [CrossRef]
33. Hrnčič, M.K.; Škerget, M.; Knez, Ž. Density and viscosity of the binary polyethylene glycol/CO_2 systems. *J. Supercrit. Fluids* **2014**, *95*, 641–668. [CrossRef]
34. Ben Said, A.; Guinot, C.; Ruiz, J.-C.; Grandjean, A.; Dole, P.; Joly, C.; Chalamet, Y. Modeling of supercritical CO_2 extraction of contaminants from post-consumer polypropylene: Solubilities and diffusion coefficients in swollen polymer at varying pressure and temperature conditions. *Chem. Eng. Res. Des.* **2017**, *117*, 95–109. [CrossRef]
35. Barrenechea, G.R.; Knobloch, P. Analysis of a group finite element formulation. *Appl. Numer. Math.* **2017**, *118*, 238–248. [CrossRef]